The Astrophysical Journal, 745:24 (10pp), 2012 January 20 doi:10.1088/0004-637X/745/1/24

A SEARCH FOR SEPARATED FRINGE PACKET BINARIES USING THE CHARA ARRAY

Deepak Raghavan[1], Chris D. Farrington[2], Theo A. ten Brummelaar[2], Harold A. McAlister[1], Stephen T. Ridgway[3], Laszlo Sturmann[2], Judit Sturmann[2], and Nils H. Turner[2]
[1] Center for High Angular Resolution Astronomy, Georgia State University, P.O. Box 3969, Atlanta, GA 30302-3969, USA; raghavan@chara.gsu.edu
[2] The CHARA Array, Mount Wilson Observatory, Mount Wilson, CA 91023, USA
[3] National Optical Astronomy Observatory, P.O. Box 26732, Tucson, AZ 85726-6732, USA
Received 2011 August 2; accepted 2011 September 22; published 2011 December 28

ABSTRACT

We present the results of a comprehensive search for new companions to nearby solar-type stars using the separated fringe packet (SFP) technique at the Center for High Angular Resolution Astronomy (CHARA) Array. Our search included 636 observations of 186 stars, searching for companions with separations of approximately 8–80 mas and moderate brightness ratios ($\Delta K \lesssim 1.5$). This survey was undertaken to support a comprehensive assessment of companions to solar-type stars within 25 pc. We detected separated fringe companions to two stars (HD 3196 and 79096) and found faint companion signatures to two more stars (HD 98231 and 137763). All of these companions are previously known by spectroscopic methods, and three of them have speckle interferometric observations as well. The faint companion seen to HD 98231 represents the first visual detection of this spectroscopic companion. Our null detection for new companions implies that the presumed gap between spectroscopic and visual techniques has largely been filled for nearby solar-type stars, thanks to systematic radial-velocity observations over multiple decades and a thorough coverage using visual techniques, especially speckle interferometric observations. We also generate simulated fringe packets to derive detection limits for SFP binaries using the CHARA Array.

Key words: binaries: visual – solar neighborhood – stars: solar-type – surveys – techniques: interferometric

Online-only material: machine-readable table

1. INTRODUCTION

Comprehensive surveys of stellar multiplicity provide important clues about star formation and evolution. The wide ranges in binary separations and magnitude differences require the use of many different techniques in order to ensure a thorough coverage of the parameter space. The shortest-period systems are effectively surveyed by spectroscopic techniques, which are typically limited to characterizing binaries with orbital periods shorter than, or of the order of, the duration of the radial-velocity monitoring. The more widely separated binaries are addressed by a variety of specialized visual observations. Coronagraphic and adaptive optics (AO) searches using telescopes of apertures as large as 10 m are effective in revealing high-contrast binaries with separations down to about 100 mas (Roberts et al. 2005; Chauvin et al. 2006; Metchev & Hillenbrand 2009; Janson et al. 2011). Speckle interferometry, while limited by relatively modest contrast limits, has enabled the identification of companions down to the diffraction limit of ground-based telescopes (e.g., Mason et al. 2001; Hartkopf et al. 2008). Recent improvements to this technique such as the use of electron-multiplication CCD cameras on telescopes of apertures up to 6 m have improved sensitivity and contrast to $V \lesssim 16$ and $\Delta m \lesssim 6$ (Tokovinin et al. 2010; Docobo et al. 2010), and enhanced data processing techniques such as fitting the shape of the speckle transfer function using reliable two-color speckle photometry have enabled separation detection down to about one-quarter of the diffraction limit (Horch et al. 2011). Finally, the most widely separated companions are revealed by common proper motion analyses. Could the well-established techniques mentioned above leave a gap in detection space, namely, companions too close to be detected by the visual methods and too wide to be addressed by spectroscopic surveys? Such a gap has long been recognized (McAlister 1976), and identified more recently in AO and speckle interferometric surveys (Bouvier et al. 1997; Mason et al. 1998). The current effort addresses this question for nearby solar-type stars using the separated fringe packet (SFP) technique at the Center for High Angular Resolution Astronomy (CHARA) Array (ten Brummelaar et al. 2005). The summary results of this search were included in the comprehensive companion assessment to solar-type stars presented in Raghavan et al. (2010), while the details are presented here.

The primary use of long-baseline interferometers in the study of binary stars is to make calibrated visibility measurements in order to derive visual orbits for known spectroscopic pairs, thereby yielding full orbital solutions and mass estimates (e.g., Hummel et al. 1993; Boden et al. 1999; Raghavan et al. 2009). In these observations, a seemingly single interference fringe contains information on the stellar and orbital properties of the pair during the epoch of observation, thereby enabling a solution for these parameters from the visibility measurements. On a two-telescope beam combiner like CHARA Classic, this technique requires several bracketed observations of the science star with those of a calibration star to pick up any evidence of binarity, and is hence too time consuming to be an effective approach for the search of new binaries in large samples. Beam combiners that utilize more than two beams, thereby producing closure phases, can find evidence of binarity more quickly, but still require bracketed observations with calibrators. In this experiment, we used the two-beam system as it has much better sensitivity. With such a configuration, the SFP technique is ideally suited for large survey projects because it can reveal a binary as a pair of spatially resolved fringes with just one observation. Once a binary is discovered, additional observations on different baselines and epochs can be used to fully derive an orbital solution. The SFP method was first demonstrated by Dyck et al. (1995) at the Infrared Optical Telescope Array, and has subsequently been used at the Palomar Testbed Interferometer

(Lane & Muterspaugh 2004), and most recently, at the CHARA Array (Bagnuolo et al. 2006; Farrington et al. 2010). The primary objective of this work is to search for new companions at projected angular separations of a few tens of milliarcseconds from nearby solar-type stars using this technique and the long baselines of the CHARA Array.

2. OBSERVATIONS AND RESULTS

The sample of stars for the overall multiplicity survey supported by this effort was presented in Raghavan et al. (2010). Targets for our SFP observations represent the subset of this overall sample that is reachable by the CHARA Array: declination $\geqslant -10^{\circ}$, $V \leqslant 9$, and $K' \leqslant 6$. While ongoing updates at the Array continually improve its sensitivity, the V and K' magnitude limits used here enabled effective tip-tilt tracking of the star and adequate signal-to-noise recording of fringes, respectively, in moderate seeing conditions. These criteria yielded 288 stars, including a few widely separated companions to our sample stars that were bright enough to be investigated separately from the primary. A complementary survey using the same technique and instrument (Farrington 2008) observed 92 of these stars, leaving 196 targets for this effort.

We obtained 636 observations on 186 of these 196 stars between 2007 January and 2008 July over approximately 100 nights. All of our observations were made using two-telescope baselines and the CHARA Classic IR pupil-plane beam combiner through the K' filter as described by ten Brummelaar et al. (2005). The Array's longest baselines are well suited to probing for SFPs from companions with projected separations down to about 10 mas. On any given baseline, the separation between the two fringes of a binary depends on the orbital phase as well as the relative orientation of the stars and the baselines. In order to maximize the likelihood of detecting a companion, if present, it is best to observe the star along two roughly orthogonal baselines while the binary is in roughly the same orientation. This approach also improves the confidence of a null detection, which is equally important in a multiplicity survey. Accordingly, the vast majority of our observations were made using the S1–E1 (45%) and S1–W1 (35%) baselines, which not only are among the longest baselines of the Array with telescope separations of 331 m and 279 m, respectively, but also are roughly orthogonal. Eight (1%) of the observations were obtained on the E1–W1 baseline and the remaining 19% were gathered using intermediate baselines (S2–W1, S2–W2, S1–E2, S2–E1, S2–E2) when the longer baselines were not available to our program.

Five of the 186 stars were observed only once, and the remaining 181 were observed 2–15 times. While observations were sometimes repeated along the same direction, i.e., two observations on S1–E1 or an observation each on S1–E1 and S1–E2, coverage along different directions is important. Hence, all but 16 stars were observed along at least two directions (S–E and S–W) and all eight stars observed on E1–W1 have observations along all three directions (S–E, S–W, and E–W). On several nights, we observed a set of stars on one baseline, then switched baselines to a roughly orthogonal orientation and re-observed the same stars. This method maximizes the likelihood of detecting a companion, if present, by looking along different directions while holding the binary orientation roughly constant. Overall, 71 stars, representing 38% of the stars observed, have S1–E1 and S1–W1 observations on the same night.

The CHARA observing software moves a dither mirror back and forth across the fringe to facilitate multiple scans of the interference pattern. In the default setting, it records data until 200 scans of adequate fringe signal are obtained. For each scan, the intensity of the interference pattern within a scan window is recorded, enabling the inspection of spatially SFPs. The width of the scan window for the 2007 data is 175 μm, and for the 2008 observations is 145 μm due to implementation of hardware updates at CHARA. Data were reduced using an IDL code written by D.R., which followed the reduction procedure in a MathCAD program written by H.A.M. First, dark noise is subtracted and the beams from each side of the beam combiner are balanced using the signal recorded during the shutter sequence, i.e., when light from each and both telescopes is successively blocked. Next, a Fourier transformation of the data is obtained and "good" fringes are selected as ones with at least twice the integrated power in a 60 Hz bandwidth centered at the fringe frequency when compared to the power in a 60 Hz background window. The qualifying scans are then low-pass and bandpass filtered to reduce noise. Finally, the fringe envelope, i.e., the outline of the diffraction pattern, is generated for each scan of the image by nullifying the negative frequencies and taking twice the modulus of the inverse Fourier transform of the bandpass-filtered signal.

The inspection for SFP is facilitated by three summary fringe envelope plots, described below, as well as a visual inspection of each fringe envelope. The three summary fringe envelope plots are (1) a normalized shift-and-add of the individual fringes, with each fringe's shift determined by cross-correlating the fringe with a reference fringe; (2) a normalized sum of the autocorrelation of each fringe envelope, which produces a symmetric plot with a central peak, and when there is a separated fringe, a second peak on either side; and (3) a simple normalized shift-and-add of the fringe envelopes by aligning the peaks of each envelope. While all three plots serve the same purpose, they have some differences, and experience has shown it useful to inspect all three. For example, when two fringes are found, the first plot described above is the best for follow-up astrometry as it best preserves the directional orientation of the fringes allowing for differential brightness assessments and elimination of the 180° ambiguity of the other methods. However, the simple shift-and-add plot is often better at noise cancellation of weak side lobes that are not separate fringes, while the cross-correlation plots tend to accentuate them. Figures 1 and 2 show examples of SFPs from a binary and an apparently single star, respectively. The top three panels of the plots show the summary plots discussed above and the bottom panel shows the individual envelopes corresponding to the 14 strongest fringes as determined by their integrated fringe power.

Table 1 lists the observations, sorted by the star's HD identifier (Column 1) and the epoch of mid-exposure in MJD (Column 2). Column 3 identifies the two-telescope baseline and Column 4 lists the fringe frequency in Hertz. We used a frequency of 150 Hz in good seeing conditions, dropped it to 100 Hz for moderate seeing and to 65 Hz in a few instances of poor seeing. For all observations, the readout frequency is five times the fringe frequency to enable adequate sampling of the data. Columns 5 and 6 list the number of good and total fringe scans contained in the observation, as described above. The last column identifies detections of SFPs. As seen in the table, the vast majority of our observations yielded no SFP detections, with only four stars showing separated fringes in a total of 13 observations. All the secondary fringes detected correspond to

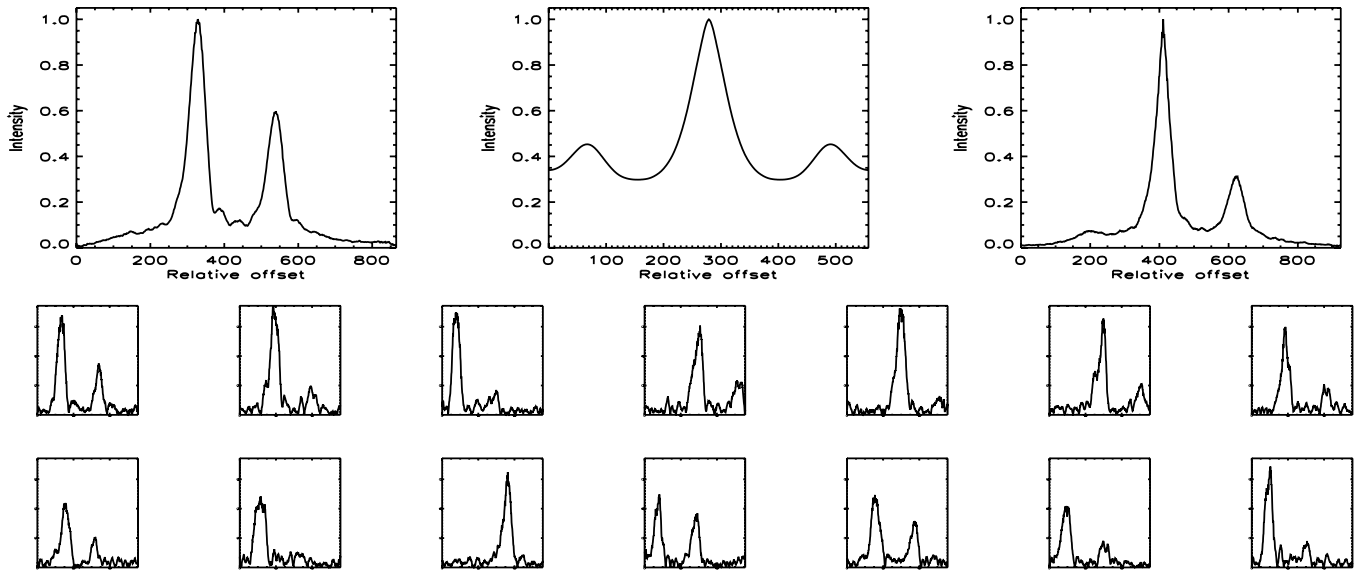

Figure 1. Example fringe envelopes of SFP detection for HD 3196, observed on MJD 54326.35 on the S1–E1 baseline. As described in the text, the summary plots in the top panel from left to right are the cross-correlation shifted sum, the autocorrelation sum, and the peak-align shifted sum, and the bottom panel shows the 14 strongest individual fringe envelopes. The *x*-axis of all plots is the relative offset in the dither mirror position as represented by the count of the sampling interval bin, and the *y*-axis is the relative intensity of the fringe envelope.

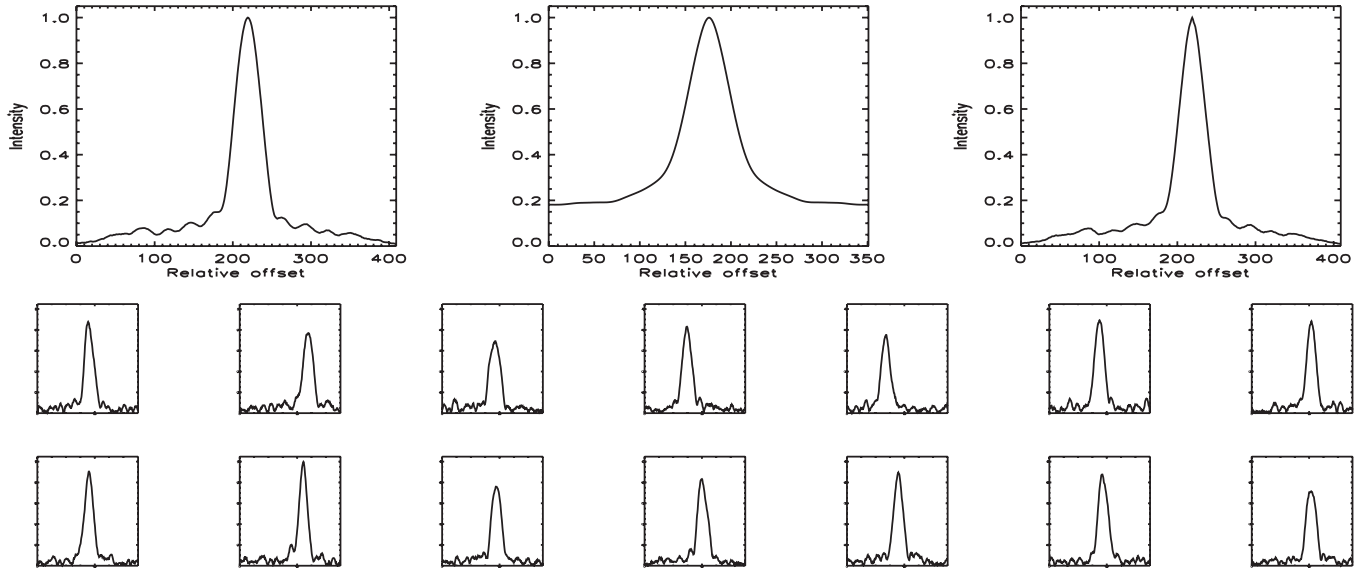

Figure 2. Example fringe envelopes for a single fringe packet star, HD 1461, observed on MJD 54674.44 on the S1–W1 baseline, in the same format as Figure 1. These plots do not show any evidence of SFPs.

previously known companions, so this effort yielded no new companions.

3. ASTROMETRY OF SEPARATED FRINGE PACKET DETECTIONS

SFPs were consistently detected for HD 3196 and 79096. HD 3196 is a hierarchical triple system composed of a 6.9 year period double-lined spectroscopic and visual binary, the primary component of which is itself a 2.1 day spectroscopic binary. We recorded separated fringes on five observations corresponding to the wider pair (see Figure 3). An additional observation of this star on MJD 54669.4208 showed evidence of just a single fringe. The secondary fringe could have been too widely separated to be recorded at this epoch, or have been hidden in the noise due to relatively poor fringe quality. HD 79096 is a 2.7 year double-lined spectroscopic and visual binary with a widely separated brown dwarf pair 43″ away. We obtained 10 observations, six of which show clear evidence of separated fringes for the stellar binary (see Figure 4). The last two observations are for each of a pair of widely separated fringes, which were too far apart to fit in the observing window. These observations show no further evidence of binarity of the individual components. The other two observations with only a single fringe are flanked by closely separated fringes, so it is likely that the baseline-binary orientation during these observations caused the two fringes to merge into one.

Hints of SFPs were seen on single observations of two more stars—HD 98231 and 137763. HD 98230/1 is the well-known quadruple system ξ UMa with claims of a fifth companion (Mason et al. 1995) that we believe is not gravitationally bound (Raghavan et al. 2010). The system is comprised of a 1.″6

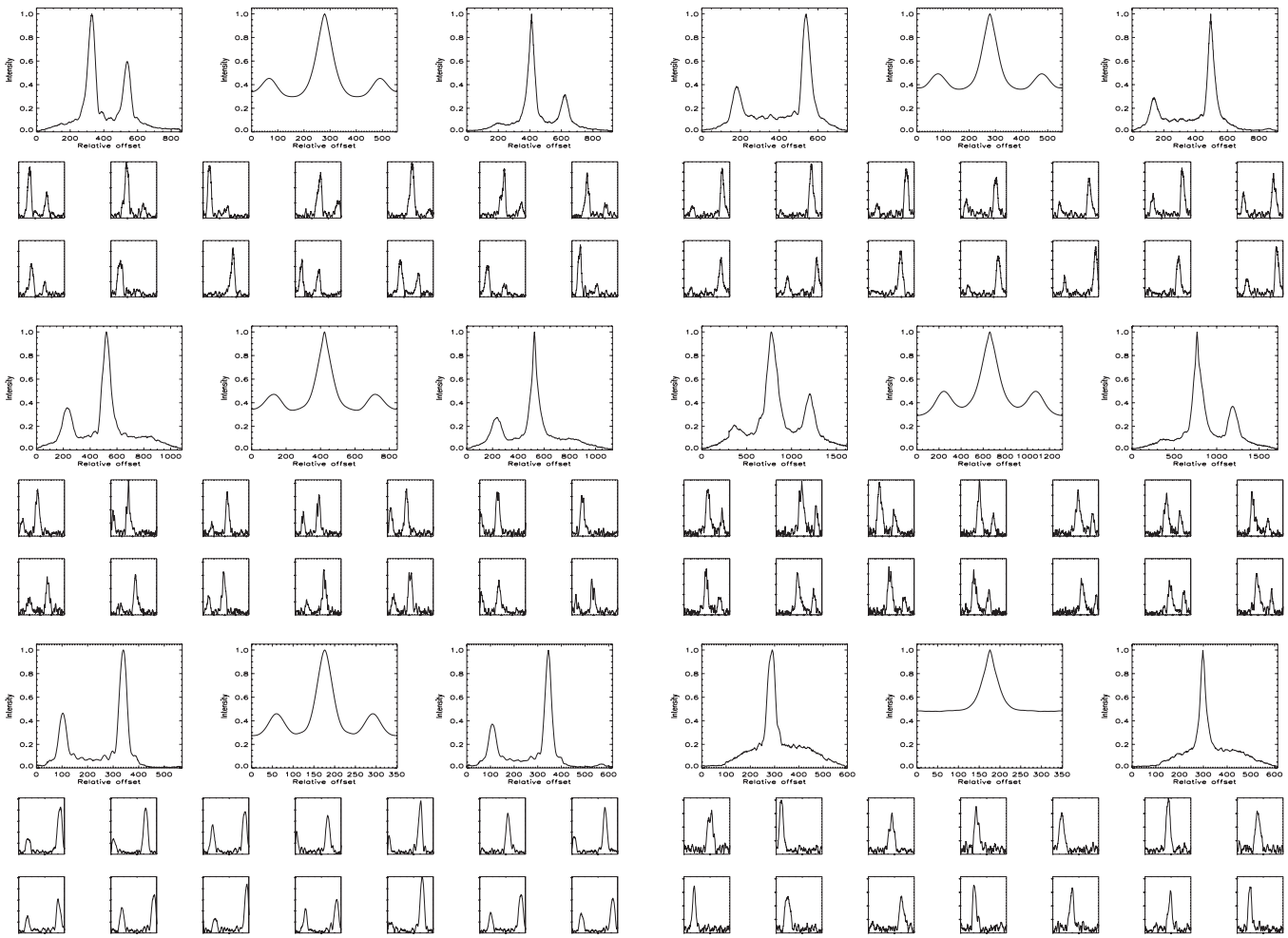

Figure 3. Fringe envelopes for HD 3196 in the same format as Figure 1, listed in observing sequence. The first five show evidence of SFPs.

Table 1
Separated Fringe Packet Observations

HD	Observation	Baseline	Fringe	Fringe Scans		SFP?
Name	MJD		Frequency	Good	Total	
000166	54310.4937	E1–S1	100	200	200	...
000166	54326.3340	E1–S1	150	198	198	...
000166	54326.4070	W1–S1	150	181	198	...
001461	54360.4082	W1–S2	65	241	241	...
001461	54669.4122	E1–S1	150	167	333	...
001461	54674.4350	W1–S1	150	202	202	...
001562	54328.4132	W1–S1	100	169	441	...
001562	54328.5041	E1–S1	100	208	327	...
001562	54655.4501	W1–S1	100	125	346	...
001562	54656.4179	E1–S1	100	82	472	...
003196	54326.3473	E1–S1	150	198	198	Yes
003196	54326.4873	W1–S1	150	197	198	Yes
003196	54360.4202	W1–S2	100	201	205	Yes
003196	54370.2520	E2–S2	65	198	198	Yes
003196	54654.4872	W1–S1	150	200	200	Yes

(This table is available in its entirety in a machine-readable form in the online journal. A portion is shown here for guidance regarding its form and content.)

visual binary, each component of which is itself a single-lined spectroscopic binary. On several observations, after finding the first fringe, we scanned a few centimeters around it with the optical path length equalizer carts and detected the second fringe from the visual binary. We recorded the data for each fringe separately to look for the spectroscopic companion and possibly for the claimed fifth companion. Given the high brightness ratios in these situations, we could not detect any

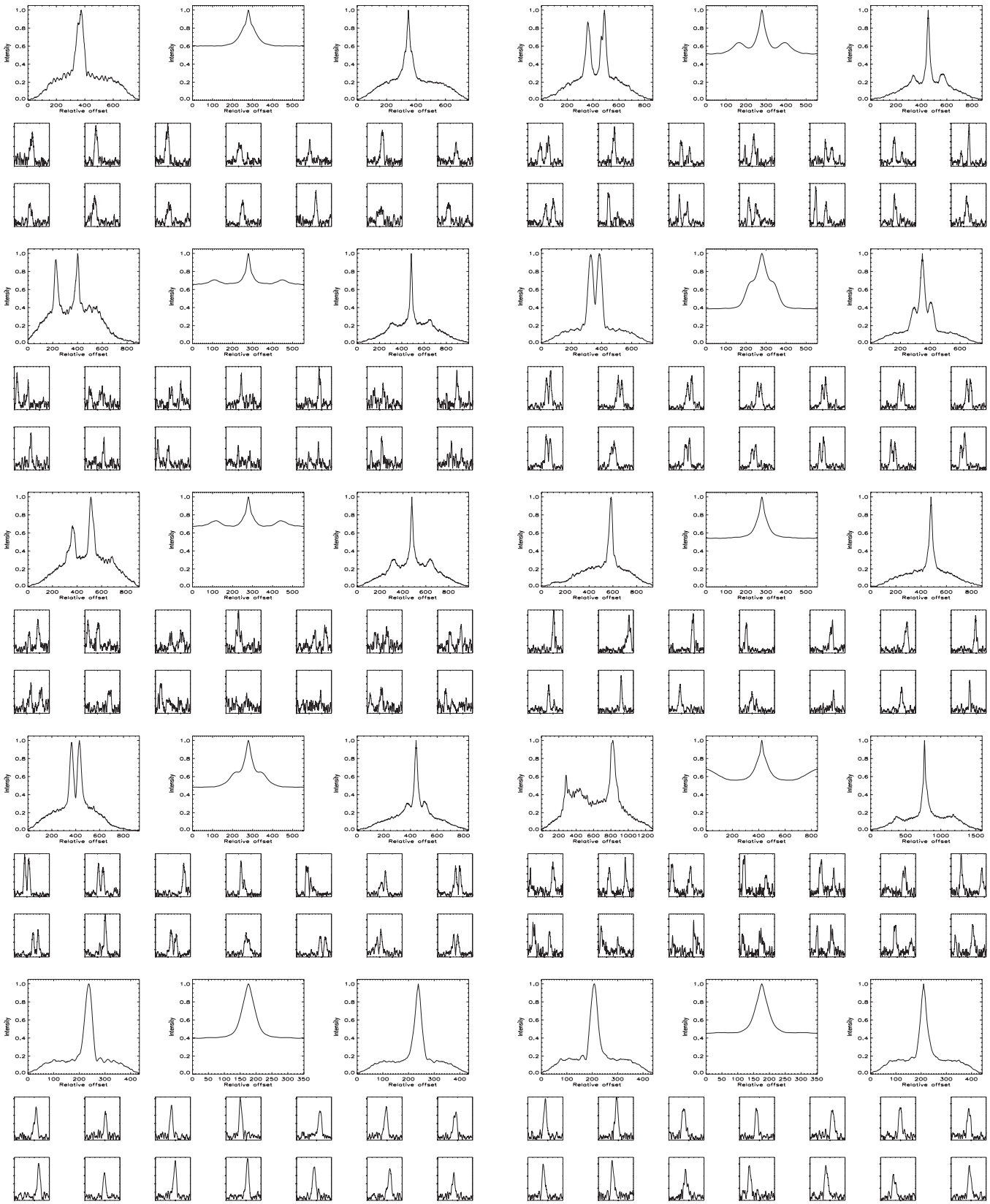

Figure 4. Fringe envelopes for HD 79096 in the same format as Figure 1, listed in the observing sequence. Six show clear evidence of SFPs, and the last two are individual observations of each component of an SFP with fringes too widely separated to fit within the observing window.

companions, although one observation on MJD 54214.3418 picks up a secondary fringe just above the noise to the right of the primary fringe, presumably corresponding to the 1.8 year spectroscopic pair that makes up the primary component of the visual binary. While this pair has well-established spectroscopic evidence as well as photocentric wobble (Heintz 1996), our

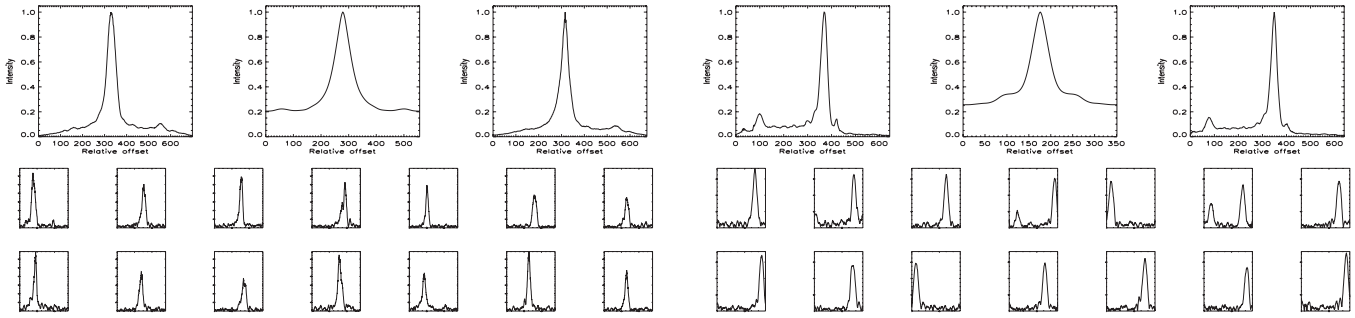

Figure 5. Marginal SFP detections for HD 98231 (left) and HD 137763 (right) in the same format as Figure 1.

Table 2
Projected Vector Separations from SFP Observations

HD Name	Observation MJD	Baseline Length (m)	Baseline Angle (deg)	Projected Separation (mas)
003196	54326.3473	321.7882	49.7	45.16
003196	54326.4873	258.5636	319.9	95.46
003196	54360.4202	244.1286	324.5	53.49
003196	54370.2520	230.3111	54.7	52.33
003196	54654.4872	189.4092	122.2	110.48
079096	54156.3715	297.2783	88.8	26.97
079096	54156.4267	301.8932	102.6	37.80
079096	54168.3331	297.5758	86.6	13.71
079096	54168.4221	308.0056	109.3	35.97
079096	54170.3343	297.2726	88.9	15.37
079096	54433.3978	248.0197	233.0	72.75
098231	54214.3418	247.4776	329.8	61.54
137763	54570.3874	213.1541	316.9	112.66

observation, if confirmed to belong to this pair, will be the first visual identification of the faint component.

HD 137763 is also a quadruple system, but arranged differently. The central pair of this system is a 2.4 year double-lined spectroscopic and visual binary, with additional distant components 52″ and 20′ away. Our observation on MJD 54570.3874 on the W1–S1 baseline suggests a faint secondary fringe, corresponding to the inner pair of the system. Figure 5 shows the results of these two observations.

Projected vector separations were derived as described in Farrington et al. (2010) for the 13 scans with double fringe packets, and the results are recorded in Table 2. Columns 1 and 2 are the same as in Table 1. Columns 3 and 4 list the projected baseline length in meters and its orientation measured in degrees from north to east, respectively. Column 5 lists the projected vector separation between the two fringes in mas. The first four observations of HD 3196 and the first five observations of HD 79096 were obtained near their respective periastron passages. Due to the rapid changes in relative positions near periastron, triangulation is reliable only for observations taken very close together in time. The first two observations of HD 3196, taken on the same night, yield a separation of 91″ at 339°, and the next two observations, taken 10 days apart, result in 71″ at 353°. While error ellipses cannot be derived from just two observations, these measurements are consistent with the published orbit for this pair (Mason & Hartkopf 2005). Similarly, the first two observations of HD 79096, taken on the same night, result in a separation of 56″ at 300°, and the next three observations, taken two days apart, yield 62″ ± 18″ at 289° ± 6°, which are all consistent with its published orbit (Mason et al. 1996).

4. SFP MODELING AND DETECTION LIMITS

In order to determine the SFP detection limits of the CHARA Array, we generated simulated fringes for a set of fictitious binaries with various separations and brightness ratios for varying atmospheric conditions. T.t.B wrote the underlying code that generates simulated data for a specified star or binary, observing parameters, and seeing conditions. Binary parameters include the visibilities of the two stars, total photon count, separation between the fringes in microns, and the brightness ratio of the two stars. Observing parameters include the telescope pair, fringe frequency, and the fringe-scan range in microns. Atmospheric conditions are modeled as described in ten Brummelaar (1996), using input seeing conditions specified as r_0, the Fried parameter, and τ_0, the timescale over which the changes in turbulence become significant. Our modeling includes piston and tip-tilt errors imposed by the atmosphere. Higher-order wavefront distortions will reduce the visibility amplitude, but not affect the astrometry of the two fringe packets. We include the effects of these higher-order modes by introducing random changes in the fringe visibility amplitudes of the two fringe packets. The output is written to a FITS file in the same format as the observing software, so it can be processed by the regular reduction pipeline.

To estimate the range of the binary's projected separation for which the Array can record separated fringes on its longest baseline within the fringe-scan window, we generated fictitious fringes for a pair of simulated G0V stars with various separations between 5 mas and 90 mas. The resulting plots from the analysis of these simulated data using the SFP detection software described in Section 2 are included in Figure 6. Projected separations of less than 8 mas cause the two fringes to overlap fully such that they resemble a single fringe, escaping SFP detection, while those of greater than 80 mas are too wide to fit within the fringe-scan window. Projected separations within these limits, i.e., 8–80 mas, can be readily detected as SFPs on the Array's longest baselines. Note that the observed projected separations are often less than the true binary separation due to a non-zero angle between the orientations of the baseline and the binary. For these and all of our other simulations, we estimated angular diameters using radii corresponding to spectral types from Cox (2000) and assuming a distance of 20 pc to the star (the median value of our 25 pc sample). Stellar visibilities were then determined assuming a baseline of 331 m (corresponding to the S1–E1 baseline) and an observing wavelength of 2.13 μm (the central wavelength of the K'-band observations). Photon counts were estimated using the $M_{K'}$ values corresponding to spectral types from Binney & Merrifield (1998), a distance of 20 pc, and

$$N_{\rm ph} = 2.37 \times 10^{(9-K)/2.5}, \quad (1)$$

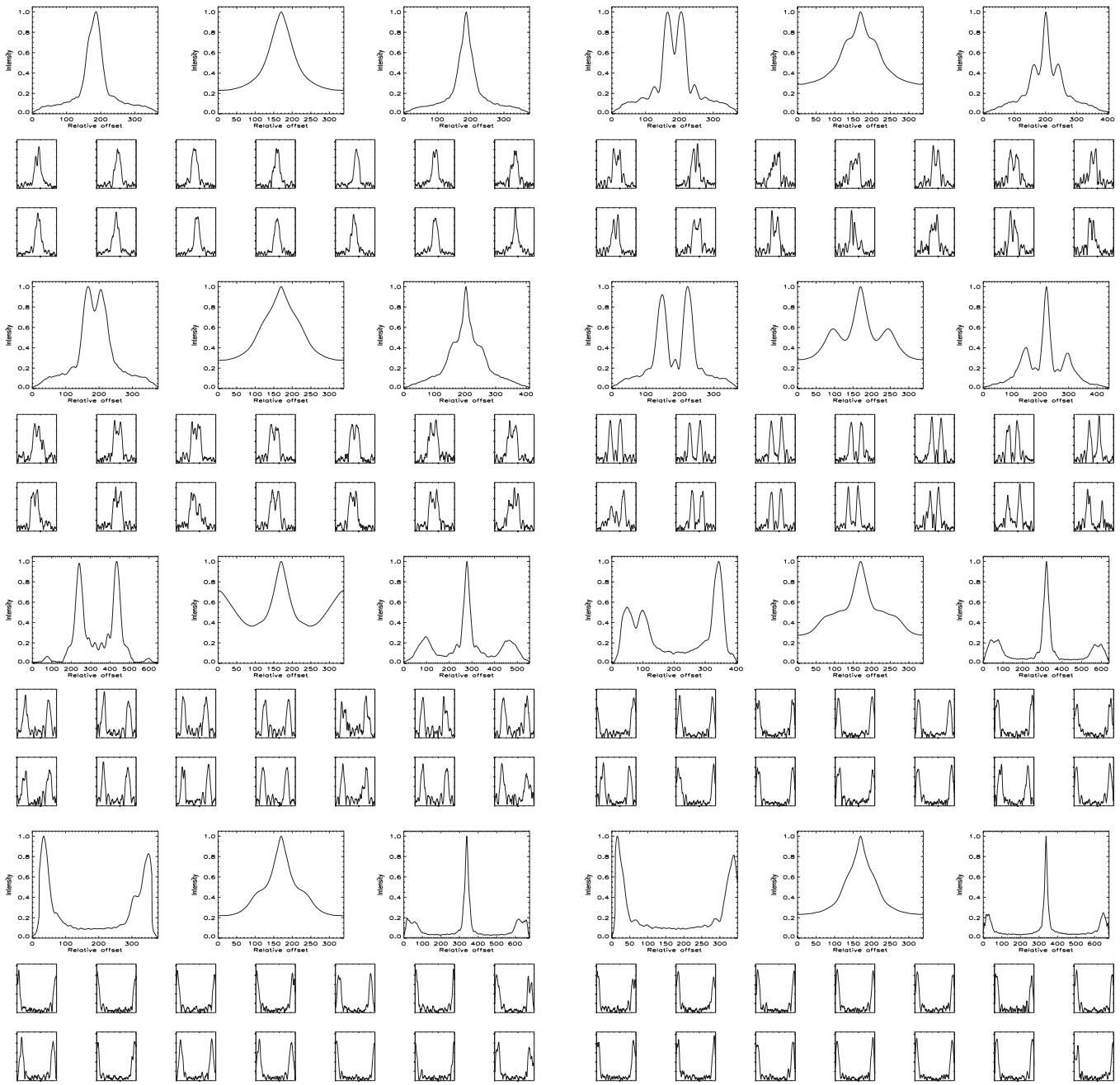

Figure 6. Model fringe envelopes for a fictitious pair of G0V stars with projected separations of 5, 8, 12, 20, 50, 70, 80, and 90 mas with simulated seeing conditions of $r_0 = 10$ cm, in the same format as Figure 1.

where we have used the approximation that for a zero-magnitude colorless star there are 4.31×10^9 photons m^{-2} s^{-1} μm^{-1} reaching the ground, and factored it for the two 1 m diameter telescopes, the same sample times as used on the sky, the bandwidth of the K' filter used on the sky, the measured throughput of the optical system, and the quantum efficiency of the detector. Fringe separation in microns was determined by multiplying the assumed projected separation in mas with the baseline length of 331 m. A fringe-scan window of 145 μm was assumed for all simulations, corresponding to the narrower value of the 2008 data. Finally, we assumed a constant wind speed for all simulations of 10 m s^{-1} in the upper layers of the atmosphere responsible for majority of the turbulence, and determined τ_0 using $\tau_0 = r_0$/wind speed. For simulations checking the effects of separation or brightness ratio, we fixed $r_0 = 10$ cm, a typical value at Mount Wilson in the summer months, corresponding to a seeing of about 1.″2 for $\lambda = 500$ nm. For r_0 below 6 cm (worse than 2″ seeing at $\lambda = 500$ nm), we assumed a fringe frequency of 500 Hz, and for better seeing conditions, we assumed a fringe frequency of 750 Hz, consistent with our observing practice.

To check the effects of varying seeing conditions on fringe quality and SFP detectability, we generated simulated fringes for a G0V–G5V pair with a projected separation of 50 mas, observed under seeing conditions varying from excellent ($r_0 =$ 20 cm, 0.″6 seeing at $\lambda = 500$ nm) to marginal ($r_0 = 3$ cm, 4″ seeing at $\lambda = 500$ nm). The output from the standard reduction code from these data is included in Figure 7. As expected, the data quality deteriorates with worsening seeing in a manner that is consistent with our experience with real data. At values of r_0 approaching 3 cm, the seeing conditions tend to smear out the

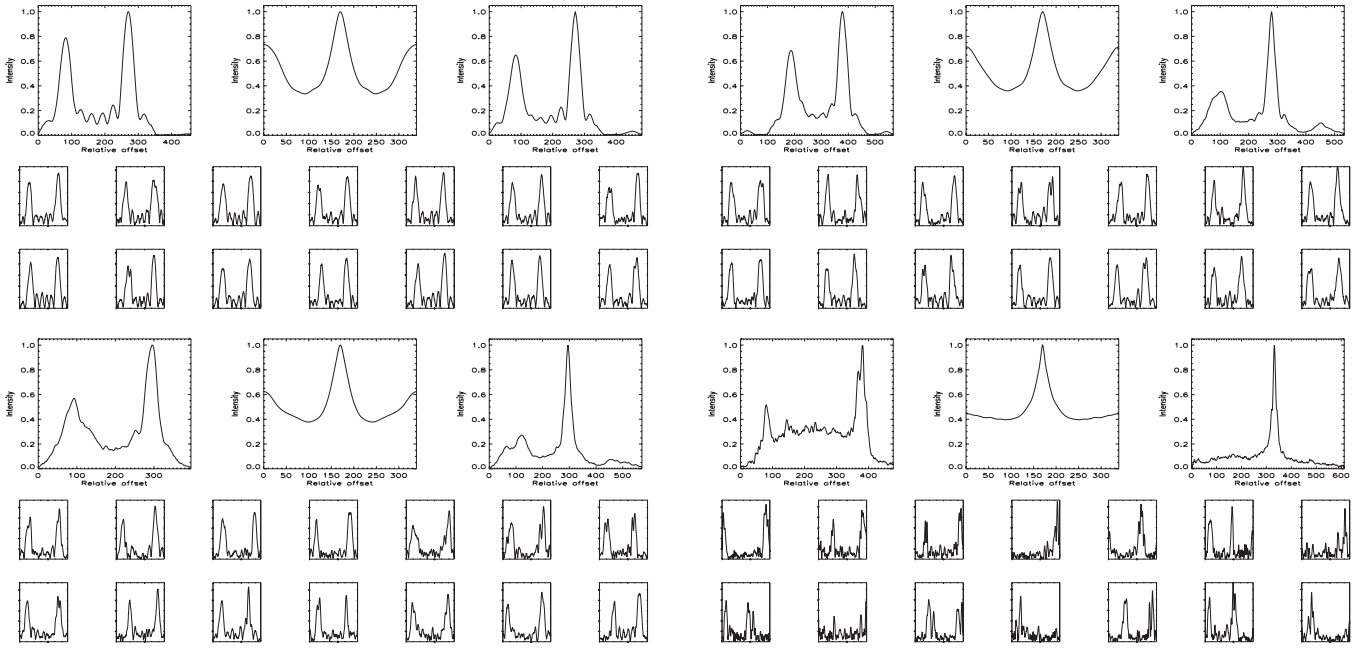

Figure 7. Model fringe envelopes for a fictitious G0V–G5V pair with a projected separation of 50 mas, in varying simulated seeing conditions of $r_0 = 20$ cm, 10 cm, 6 cm, and 3 cm, in the same format as Figure 1.

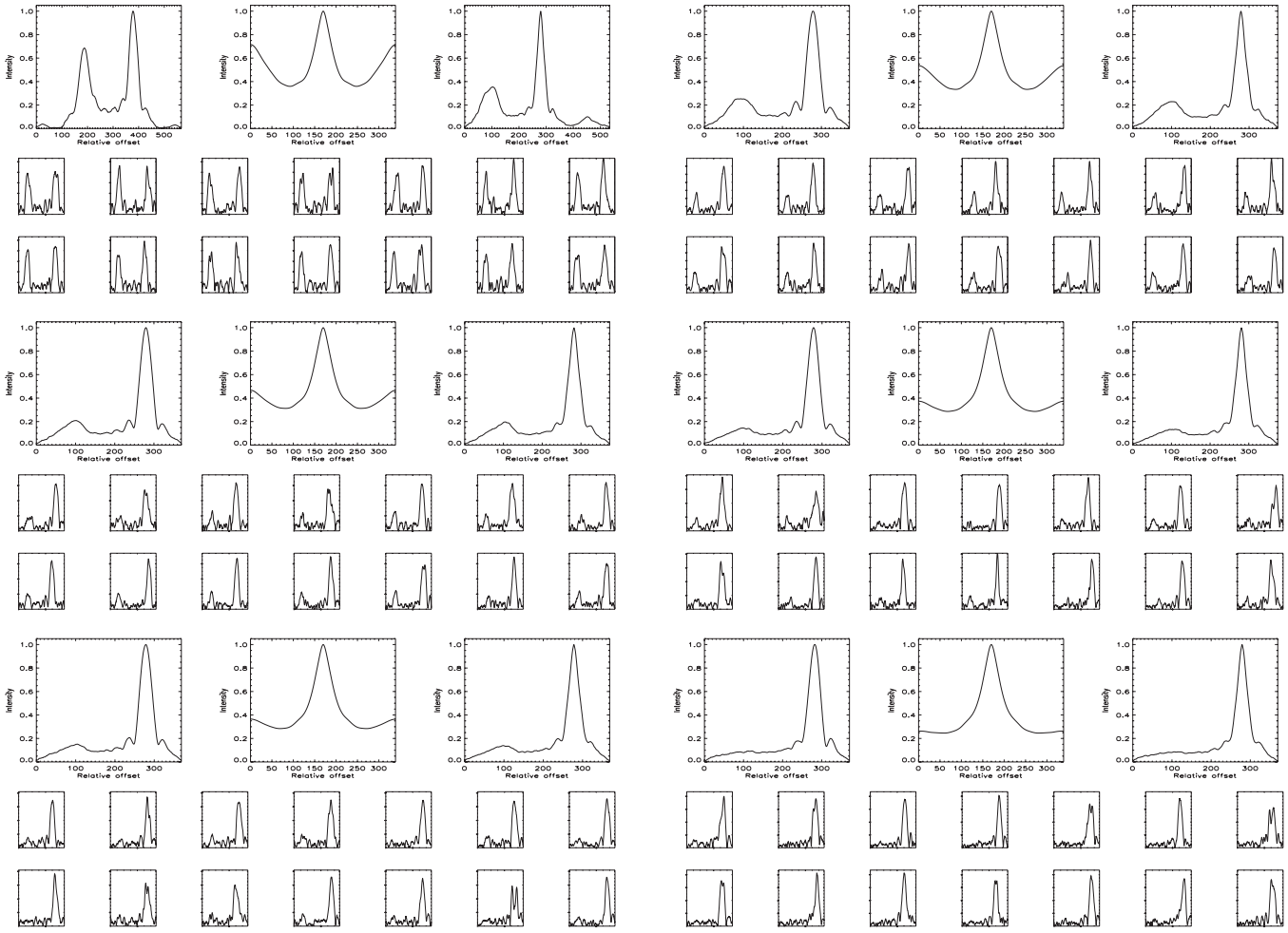

Figure 8. Model fringe envelopes for a fictitious pair of varying contrasts in the same format as Figure 1. In all plots, the primary is a G0V star, separation is 50 mas, and the simulated seeing corresponds to $r_0 = 10$ cm. The companions, in sequence, are G5V, K0V, K5V, K8V, M0V, and M2V.

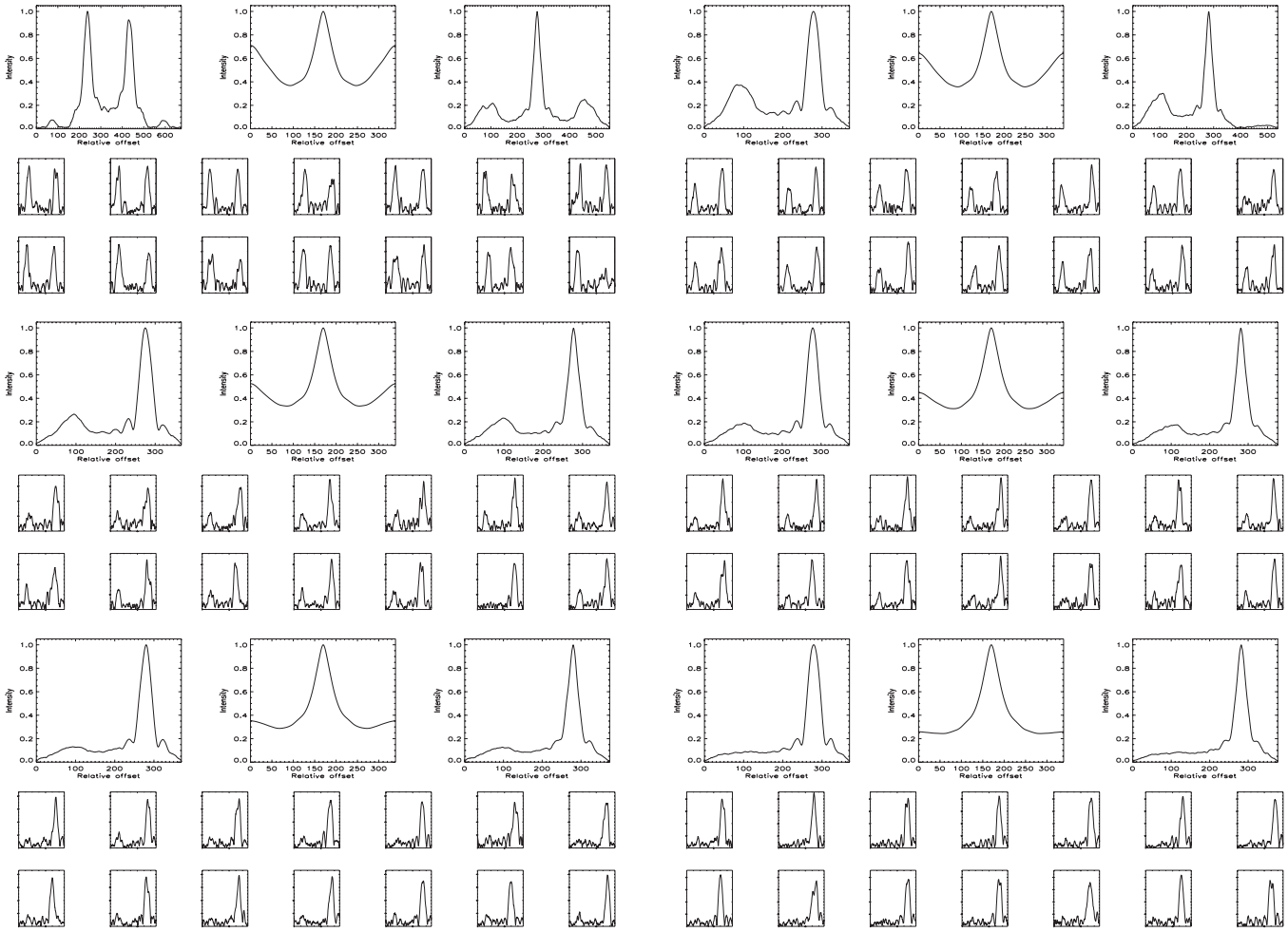

Figure 9. Model fringe envelopes for a fictitious pair of varying contrasts in the same format as Figure 1. In all plots, the primary is a G5V star, separation is 50 mas, and the simulated seeing corresponds to $r_0 = 10$ cm. The companions, in sequence, are G5V, K0V, K5V, K8V, M0V, and M2V.

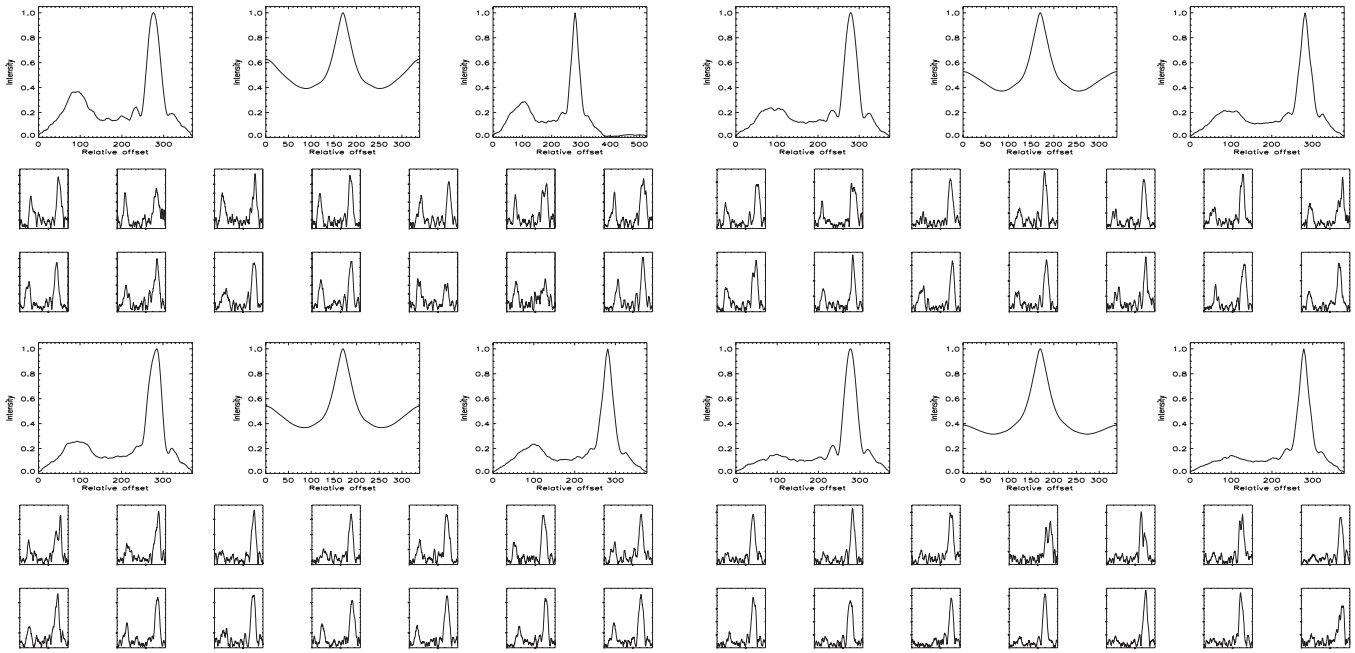

Figure 10. Model fringe envelopes for a fictitious pair of varying contrasts in the same format as Figure 1. In all plots, the primary is a K0V star, separation is 50 mas, and the simulated seeing corresponds to $r_0 = 10$ cm. The companions, in sequence, are K5V, K8V, M0V, and M2V.

secondary fringe into the noise, making detection very hard and any astrometry impossible.

Finally, to check the ΔK limit for SFP detection, we generated model fringes for binaries with primaries G0V, G5V, and K0V, and secondaries varying from the primary's spectral type, down to M2V. The resulting plots are included in Figures 8–10. For the G0V primary (Figure 8), secondaries down to M0V are detectable ($\Delta K = 2.0$), but M2V is not ($\Delta K = 2.6$). An M2V star at 20 pc will have $K \sim 7.3$, approaching the magnitude limit of the Array to detect fringes. However, fringes have been recorded for stars down to this limit, and even a bit fainter, so the relative signal strength, rather than absolute, is responsible for non-detection here. The above limits apply to relatively widely separated fringes. When the two fringes get closer, the secondary fringe envelope appears in the area of the primary fringe's side lobes. In these cases, the secondary fringe needs to be strong enough to stand above the primary's side lobes in order to be detected. As seen in Figure 8, for a G0V primary, this is true for secondaries down to K5V ($\Delta K = 1.4$). As pointed out in O'Brien et al. (2011), astrometry in such cases when the interference from side lobes is significant requires simultaneous fitting of the two fringes. Similarly, Figure 9 shows that for a G5V primary, companions down to K5V ($\Delta K = 1.1$) can be detected above side lobes, and down to M0V ($\Delta K = 1.7$) can be detected if widely separated. As seen in Figure 10, the ΔK limits are the same for a K0V primary, for which companions down to M0V ($\Delta K = 1.1$) can be detected above side lobes, and down to M2V ($\Delta K = 1.7$) can be identified if widely separated. Based on all these simulations, we conclude that for SFP detection, companions must have a K magnitude of within 1.1 of the primary to be detected unequivocally, while companions up to about half a magnitude fainter can be seen if separated widely enough to avoid interference from the primary's side lobes.

5. CONCLUSION

In this effort, we utilized the long baselines of the CHARA Array to search for previously undetected companions to solar-type stars with projected separations of about 8–80 mas. We inspected this specific range to examine the possibility of an unexplored gap between radial-velocity searches, which detect close-in companions, and traditional visual methods, specifically speckle interferometry, which have routinely detected companions down to the diffraction limit of ground-based telescopes (Mason et al. 2001; Horch et al. 2008), and recently even below these diffraction limits (Horch et al. 2011). We observed 186 stars, detecting SFP companions to only two stars (HD 3196 and 79096) and seeing hints of companions to two more (HD 98231 and 137763). All these detections correspond to previously known companions, with spectroscopic and/or visual observations. Our null detection of new companions is nevertheless useful in enabling the comprehensive companion search presented in Raghavan et al. (2010). For the well-studied sample of solar-type stars within 25 pc, we have thus verified that the putative gap in detection space between spectroscopic and visual observations has largely been filled (see Section 5.1 in Raghavan et al. 2010). To provide adequate context for our null detection, we generated simulated fringes to derive SFP detection limits for the CHARA Array. The longest baselines of the Array are capable of identifying separated fringes with projected separations of 8–80 mas for pairs with $\Delta K \lesssim 1.5$ (see Section 4 for specifics). The SFP technique remains a very efficient method of searching for companions in this parameter space, and our detection limits can aid the planning of future companion searches for other samples of stars.

We thank the CHARA Array operator P. J. Goldfinger for obtaining some of the data used here and for her able assistance of remote operations of the Array from AROC. Research at the CHARA Array is supported by the College of Arts and Sciences at Georgia State University and by the National Science Foundation through NSF grants AST-0606958 and AST-0908253. This research has made use of the SIMBAD literature database, operated at CDS, Strasbourg, France, NASA's Astrophysics Data System, and the Washington Double Star Catalog maintained by the U.S. Naval Observatory.

REFERENCES

Bagnuolo, W. G., Jr., Taylor, S. F., McAlister, H. A., et al. 2006, AJ, 131, 2695
Binney, J., & Merrifield, M. 1998, Galactic Astronomy (Princeton, NJ: Princeton Univ. Press)
Boden, A. F., Lane, B. F., Creech-Eakman, M. J., et al. 1999, ApJ, 527, 360
Bouvier, J., Rigaut, F., & Nadeau, D. 1997, A&A, 323, 139
Chauvin, G., Lagrange, A.-M., Udry, S., et al. 2006, A&A, 456, 1165
Cox, A. N. 2000, Allen's Astrophysical Quantities (New York: Springer)
Docobo, J. A., Tamazian, V. S., Balega, Y. Y., & Melikian, N. D. 2010, AJ, 140, 1078
Dyck, H. M., Benson, J. A., & Schloerb, F. P. 1995, AJ, 110, 1433
Farrington, C. 2008, PhD thesis, Georgia State Univ.
Farrington, C. D., ten Brummelaar, T. A., Mason, B. D., et al. 2010, AJ, 139, 2308
Hartkopf, W. I., Mason, B. D., & Rafferty, T. J. 2008, AJ, 135, 1334
Heintz, W. D. 1996, AJ, 111, 408
Horch, E. P., van Altena, W. F., Cyr, W. M., et al. 2008, AJ, 136, 312
Horch, E. P., van Altena, W. F., Howell, S. B., Sherry, W. H., & Ciardi, D. R. 2011, AJ, 141, 180
Hummel, C. A., Armstrong, J. T., Quirrenbach, A., et al. 1993, AJ, 106, 2486
Janson, M., Bonavita, M., Klahr, H., et al. 2011, ApJ, 736, 89
Lane, B. F., & Muterspaugh, M. W. 2004, ApJ, 601, 1129
Mason, B. D., Gies, D. R., Hartkopf, W. I., et al. 1998, AJ, 115, 821
Mason, B. D., & Hartkopf, W. I. 2005, IAU Comm. 26 Circ., 156, 1
Mason, B. D., Hartkopf, W. I., Holdenried, E. R., & Rafferty, T. J. 2001, AJ, 121, 3224
Mason, B. D., McAlister, H. A., & Hartkopf, W. I. 1996, AJ, 112, 276
Mason, B. D., McAlister, H. A., Hartkopf, W. I., & Shara, M. M. 1995, AJ, 109, 332
McAlister, H. A. 1976, PASP, 88, 317
Metchev, S. A., & Hillenbrand, L. A. 2009, ApJS, 181, 62
O'Brien, D. P., McAlister, H. A., Raghavan, D., et al. 2011, ApJ, 728, 111
Raghavan, D., McAlister, H. A., Henry, T. J., et al. 2010, ApJS, 190, 1
Raghavan, D., McAlister, H. A., Torres, G., et al. 2009, ApJ, 690, 394
Roberts, L. C., Jr., Turner, N. H., Bradford, L. W., et al. 2005, AJ, 130, 2262
ten Brummelaar, T. A. 1996, Opt. Commun., 132, 329
ten Brummelaar, T. A., McAlister, H. A., Ridgway, S. T., et al. 2005, ApJ, 628, 453
Tokovinin, A., Mason, B. D., & Hartkopf, W. I. 2010, AJ, 139, 743